Resistance of geopolymer and Portland cement based systems to silage effluent attack

Aiken, T. A., Sha, W., Kwasny, J., & Soutsos, M. N. (2017). Resistance of geopolymer and Portland cement based systems to silage effluent attack. DOI: 10.1016/j.cemconres.2016.11.015

Published in:
Cement and Concrete Research

Document Version:
Peer reviewed version

Resistance of geopolymer and Portland cement based systems to silage effluent attack

Authors: Timothy A Aiken[1], Wei Sha[1], Jacek Kwasny[1], Marios N Soutsos[1]
[1]School of Natural and Built Environment, Queen's University Belfast, Belfast, BT9 5AG, UK

Abstract:
Traditional Portland cement (PC) concrete has been used for many years in the agricultural industry for the construction of silos and silage effluent storage facilities. However, the acidic nature of the silage effluent produced by silage has led to severe degradation of PC concrete which in turn has significant environmental and financial implications. This study compares the resistance of PC and geopolymer (GP) mortars and pastes to silage effluent over 12 months. The GP samples displayed increased resistance to silage effluent in terms of mass and strength loss. Analysis of microstructure suggests that the increased stability of the reaction products is the main factor behind increased silage effluent resistance when compared with PC. It was also found that pulverised fuel ash (PFA) and ground granulated blast furnace slag (GGBS) blends with a higher PFA content may offer increased long term silage effluent resistance due to the nature of the main binder gel produced in PFA dominant systems.

Keywords: Organic Acids (D), Fly-Ash (D), Ground Granulated Blast-Furnace Slag (D), Microstructure (B), Durability (C)

1. Introduction
Within the agricultural industry silage effluent is known to cause damage and deterioration to concrete structures such as silo walls, floors and storage tanks [1]. Silage effluent is produced as a result of storing grass as winter feed for livestock [2]. The grass is placed in concrete silos, compacted and sealed. It then undergoes a fermentation process converting sugars to acids and producing silage effluent [3]. The resulting effluent typically contains lactic and acetic acid and has a pH value of approximately 4.0 [4], [5] and [6]. The concentration of lactic and acetic acid in silage effluent is typically in the range of 5-44 g/l and 1-5.5 g/l respectively [7]. In recent years the practice is to allow the grass to wilt or dry out as much as possible before storage. This means there is less effluent produced during fermentation because there is less moisture available [8]. Although this has helped reduce the volume of effluent produced, the problem has not been eliminated because the reduced effluent volume can still be sufficient to cause significant concrete damage. Furthermore it is not always possible to allow grass to wilt before storage due to unpredictable weather and time constraints [8].

Portland cement (PC) concrete structures have been suffering serious degradation due to effluent attack for many years. This degradation process has been observed to erode concrete progressively and may be accelerated by mechanical actions such as high pressure cleaning and machine traffic [9]. The reactions between the acidic effluent and cement hydrates produce calcium salts which are highly soluble [10]. This allows the porosity of the matrix to increase and the mechanical strength to decrease while at the same time the concrete cover is being degraded which may lead to corrosion of steel reinforcement and structures being destroyed [11]. There are significant environmental and financial consequences of such damage [9]. The escape of silage effluent can result in serious surface and groundwater pollution [8]. Silage effluent must be effectively managed and collected because it poses a considerable pollution threat [12]. Silage effluent has a biochemical oxygen demand of up to 200 times that of domestic sewage and has the potential to kill large quantities of aquatic life [13]. When this type of pollution occurs, significant financial penalties can be incurred as well as the cost to repair or reconstruct damaged

storage facilities which allowed the silage effluent to escape. Therefore there is a need for alternative materials which provide increased resistance to silage effluent attack.

Global issues such as climate change, the depletion of the earth's resources and pollution are causing many countries to commit to reducing their environmental impact specifically their CO_2 emissions [14]. The production of Portland cement is an energy intensive process [15] and approximately 0.7 – 1.1 tonnes of CO_2 are emitted for every tonne of cement produced [16]. As a result the cement industry contributes approximately 7% of worldwide CO_2 emissions [17]. However the use of alternative binder materials can reduce CO_2 emissions associated with concrete production. The use of replacement materials such as pulverised fuel ash (PFA) and ground granulated blast furnace slag (GGBS) in place of PC is estimated to reduce CO_2 emissions associated with concrete by up to 80% [18]. GGBS is obtained from the production of iron and is widely used in the production of alkali activated cements [19]. PFA is a residue obtained from coal combustion at power plants and is also considered an environmentally friendly source material [20]. However PFA is increasingly considered a valuable material. In 2014, 70% of the PFA produced in the UK was used in the manufacture of construction materials [21]. Nonetheless there are approximately 114 million tonnes of PFA stockpiled accessibly in the UK [22] and in many countries around the world utilisation of PFA is a major problem with as little as 7% being utilised effectively [23].

Individually alkali activated GGBS and alkali activated PFA have been studied by many authors. The acid resistance of these two binder types has also received much attention [24], [25], [26], [27] and [28]. More recently the possibility of blending two waste or by-products together to form one binder has been investigated [29]. Therefore the acid resistance of blended PFA and GGBS binders is less well known. Furthermore the resistance of PFA and GGBS based geopolymer (GP) cements and concretes to silage effluent attack has received very little attention within the research community. However a study was carried out recently which suggests that alkali activated GGBS displays increased resistance to organic acid collected from silos compared with traditional PC [30].

In this study two blends of GP mortars and pastes using PFA and GGBS as binder materials have been exposed to silage effluent for 12 months. PC samples have also been studied in order to compare performance and investigate the mechanism of attack on each binder.

2. Experimental methods

To investigate the resistance of GP and PC based systems to silage effluent attack, mortar samples were prepared and submerged in silage effluent for 12 months. The samples were monitored visually and their mass change and compressive strength was also recorded. Control samples were submerged in water for 2 months for compressive strength comparison. Paste samples were also prepared and submerged in silage effluent for 12 months in order to carry out microstructural analysis to gain an understanding of the mechanism of attack. The paste samples were analysed by X-ray diffraction (XRD), thermogravimetric analysis (TGA), Fourier transform infrared spectroscopy (FTIR) and scanning electron microscopy (SEM).

2.1 Materials

The PFA used in this study is a class F fly ash sourced from Power Minerals Ltd, UK and the GGBS was supplied by Hanson group, UK. Portland cement CEM I 42.5N, produced by Quinn Cement in Northern Ireland, and conforming to the standards of BS EN197-1:2011 [31] was used as PC. The oxide compositions for PFA, GGBS and PC obtained by X-ray fluorescence (XRF) are displayed in Table 1. The

XRD spectra of the binder materials PFA, GGBS and PC are shown in Figure 1. The main crystalline phases present in PFA include quartz, mullite and hematite. However, GGBS is almost completely amorphous with a broad peak or hump between (2θ) 25 and 35°. The PC used in this study has many crystalline phases including alite, belite, aluminate, brownmillerite and gypsum. The PFA and GGBS binders were activated by solutions of sodium silicate and sodium hydroxide. The sodium silicate solution was supplied by Fisher Scientific and consisted of 12.8% Na_2O, 25.5% SiO_2 and 61.7% water. The sodium hydroxide solution was prepared at 30% w/w by the dissolution of solid commercial grade (99% purity) sodium hydroxide which was allowed to cool to room temperature prior to preparation of the samples. The aggregate used was a silicate sand abundant in quartz, sourced locally in Northern Ireland. It has an oven-dry particle density of 2695 kg/m^3 and a water absorption of 0.92 and 1% after 1 and 24 hours respectively. Both density and water absorption were determined according to BS 812-2:1995 [32].

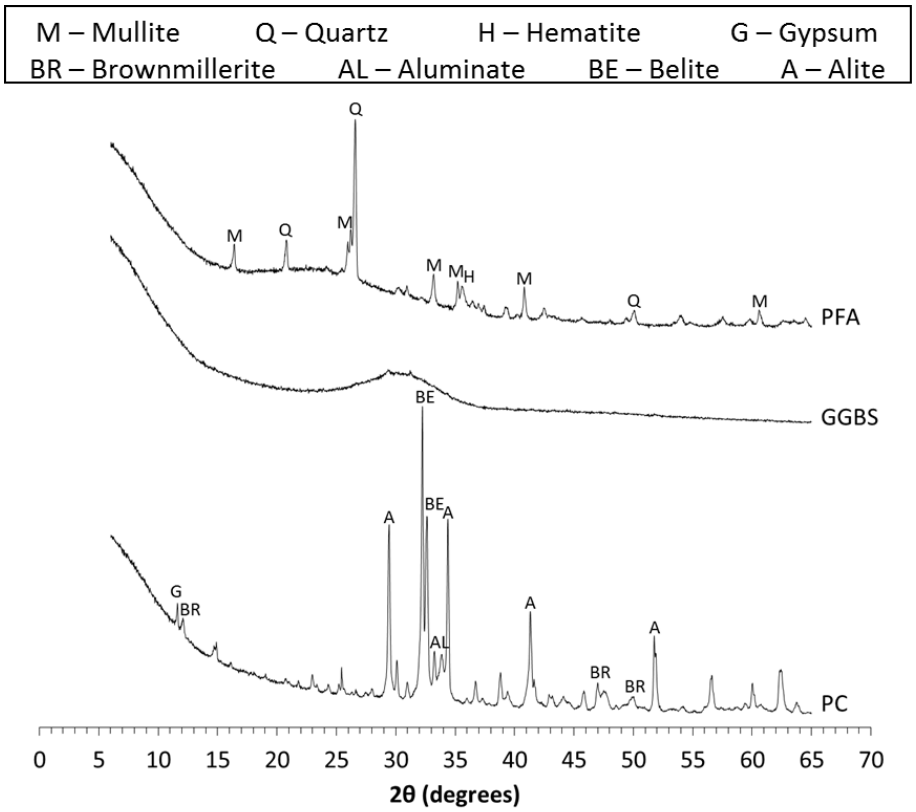

Figure 1: XRD spectra for raw materials - PFA, GGBS and PC

Table 1: Oxide compositions obtained by XRF for raw materials - PFA, GGBS and PC

Material	CaO	SiO_2	Al_2O_3	Fe_2O_3	Na_2O	K_2O	SO_3	MgO	TiO_2	MnO	LOI
PFA	2.24	46.78	22.52	9.15	0.89	4.09	0.90	1.33	1.05	0.05	3.57
GGBS	43.72	29.38	11.23	0.36	1.05	0.93	1.76	6.94	0.67	0.51	2.40
PC	63.01	20.21	4.79	2.78	0.19	0.59	2.60	1.93	0.27	0.08	3.16

2.2 Mixing, casting, curing and testing procedures

All mortar and paste mixes were prepared using a mortar mixer with a 5 litre capacity. The sand and binder component of each mix were placed in the mixer first and mixed together for one minute. The appropriate water and activating solutions were then added and mixing continued for a further five minutes. The sand to binder ratio was kept constant for all mortar mixes to allow comparison between GP and PC specimens. The mix proportions used are shown in Table 2 and are based on mix design

optimisation carried out by Rafeet and Vinai *et al.* as part of the SUS-CON project [33] and [34]. The water/solid ratio is calculated from the ratio of water to binder content (PFA and GGBS) and also includes the solid and water proportions of the activating solutions. In this study the water/solid and water/cement ratios were kept constant for mortar and paste samples to ensure the hydration/reaction products were consistent for both mortar and paste samples.

Table 2: Paste and mortar mix proportions

Mix composition		**Mortars**			**Pastes**		
		GPm-A	**GPm-B**	**PCm**	**GPp-A**	**GPp-B**	**PCp**
Binder compositions	PFA (%)	30	60	-	30	60	-
	GGBS (%)	70	40	-	70	40	-
	PC (%)	-	-	100	-	-	100
Sand/binder ratio		2.75	2.75	2.75	-	-	-
Water/solid ratio		0.42	0.40	-	0.42	0.40	-
Water/cement ratio		-	-	0.50	-	-	0.50
PFA (kg/m^3)		158	317	-	343	687	-
GGBS (kg/m^3)		369	211	-	800	458	-
PC (kg/m^3)		-	-	544	-	-	1223
Sodium silicate (kg/m^3)		124	124	-	269	269	-
Sodium hydroxide (kg/m^3)		102	102	-	221	221	-
Water (kg/m^3)		104	92	271	226	200	612
Sand (kg/m^3)		1450	1450	1495	-	-	-

The mortar and paste cubes were cast in two layers into 50 mm three-gang moulds and each layer was compacted using a vibrating table. The mortar and paste samples were demoulded after 24 hours and cured for 28 days at room temperature (20 ± 1 ^{o}C) and a relative humidity of greater than 90%.

Following curing the mortar and paste samples were submerged in raw silage effluent. The effluent volume per sample was 0.3 l and the effluent pH was approximately 4.1. The concentration of metals and anions in the raw silage effluent was determined by inductively coupled plasma mass spectrometry and ion chromatogophraphy respectively and is shown in Tables 3 and 4. The silage effluent was replaced with fresh silage effluent weekly during the first two months of submersion. After two months it was replaced monthly until 6 months. After 6 months it was replaced at 8 and 10 months. The mortar samples were inspected visually and the mass loss was recorded after 2, 5 and 12 months of submersion. When measuring the samples mass they were removed from the effluent briefly and gently dried by hand before measurements began. The samples were placed in the same orientation for the entire submersion duration. Control mortar samples from each mix were submerged in water for 2 months and the compressive strength determined. The compressive strength of the samples submerged in silage effluent was determined after 2 and 12 months. For determining mass and compressive strength four cubes were tested to obtain an average reading and the reduced cross-section due to the corroded surface layer was also considered for compressive strength calculations. To ensure consistency, protective soft board was used on the loading zones of each sample during the compressive strength tests to minimise the effect of the corroded surface layer. Microstructural analysis was carried out on the paste samples to identify the mechanism of attack by comparing the outside layer of the cube which was in direct contact with the silage effluent with the centre of the cube which was not in contact with the

silage effluent. Powdered samples were obtained by crushing the outside layer and the centre separately using a pestle and mortar. The following analytical techniques were used:

- X-ray diffraction (XRD) with PANalytical X'Pert PRO diffractometer applying CuK_{α} radiation of wavelength 1.541874 Å . Diffraction patterns were collected between 5^{o} and 65^{o} 2θ with a step size of 0.017^{o}. PANalytical X'Pert Highscore software with the powder diffraction file database was used to analyse the diffraction patterns.
- Thermogravimetric analysis (TGA) using Netzsch's TG 209. The temperature was increased up to 1000 ^{o}C at a rate of 20 ^{o}C/min in a nitrogen environment. The weight loss information obtained from the TG curve and first derivative (DTG) was used to confirm the type of hydrates and reaction products.
- Fourier transform infrared spectroscopy (FTIR) using Jacso 4100 series FTIR Spectrometer with attenuated total reflectance attachment. The spectra were gathered between 650 and 4000 cm^{-1} wavenumber at 8 cm^{-1} resolution.
- Scanning electron microscopy (SEM) with energy dispersive X-ray (EDX) analysis. The equipment used was QUANTA FEG250 with OXFORD X-Act as chemical composition analyser. EDX was run by Aztec version 2.0 software for chemical composition analysis. Paste samples were sectioned and polished carefully in preparation for SEM and EDX analysis.

Table 3: Metal concentrations of silage effluent

Metal	Concentration (mg/l)
Aluminium	4.9
Boron	0.93
Barium	1.1
Calcium	672
Cobalt	0.02
Chromium	0.14
Copper	0.48
Iron	89
Potassium	2635
Magnesium	294
Manganese	27
Sodium	551
Nickel	0.05
Silicon	51
Strontium	3.4
Titanium	0.19
Zinc	3.7

Table 4: Anion concentrations of silage effluent

Anion	Concentration (ppm)
Chloride	10651
Nitrate	432
Phosphate	5154
Sulphate	1293

3. Results and discussion

3.1 Visual appearance

Figure 2 displays the mortar samples after 12 months of submersion in silage effluent, samples submerged in water for two months are also displayed. Initially the PC sample has a much lighter grey colour than both GP samples. GPm-B is slightly darker than GPm-A due to the higher PFA content which is dark grey compared with GGBS which is white. The submersion in silage effluent has caused significant discolouration to all samples. They have become darker in colour and display some gold coloured stains. There also appears to be more visible pores which look like 'pin holes' on the samples surface compared with the samples submerged in water. For PC there is also the formation of small amounts of an additional white coloured compound on the sample surface. Paste samples (Figure 3) were also submerged in silage effluent for 12 months to carry out microstructural analysis. The formation of an additional compound is also evident on the surface of the PC paste samples and is discussed further in section 3.4.

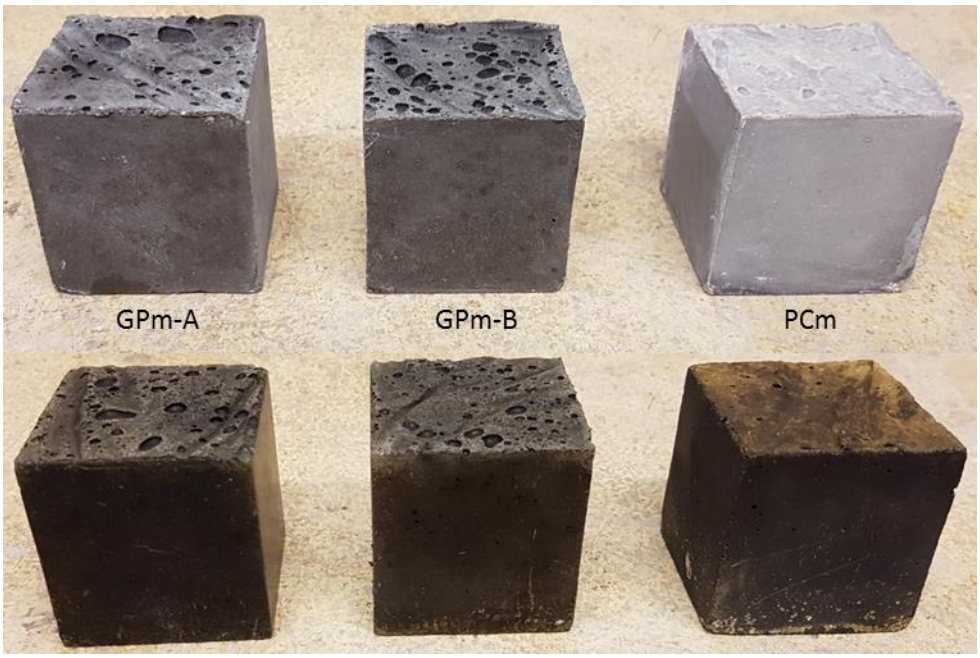

Figure 2: Mortar samples after and 2 months in submersion in water (top) and 12 months submersion in silage effluent (bottom)

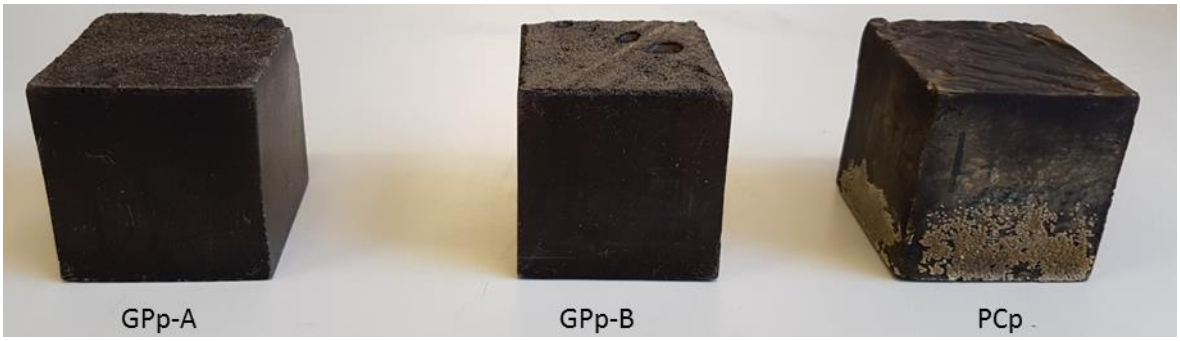

Figure 3: Paste samples after 12 months submersion in silage effluent

Figure 4 shows a slice through the paste samples submerged in silage effluent for 12 months. All of the samples display different layers of discolouration with change in depth towards the centre. These layers are similar to those identified by Bertron *et al.* (2005) [35] where three zones are described. Zone 1 is

described as the sound zone which is unaltered by the attack. Zone 2 is typically light grey in colour and can be described as a transition zone where moderate chemical changes may occur [36]. Zone 3 is described as the altered zone where significant chemical and strength changes are expected. It appears from Figure 4 that the silage effluent has caused thicker zones of deterioration in sample GPp-B. This is likely due to higher porosity reported in mixes with a higher PFA content [37].

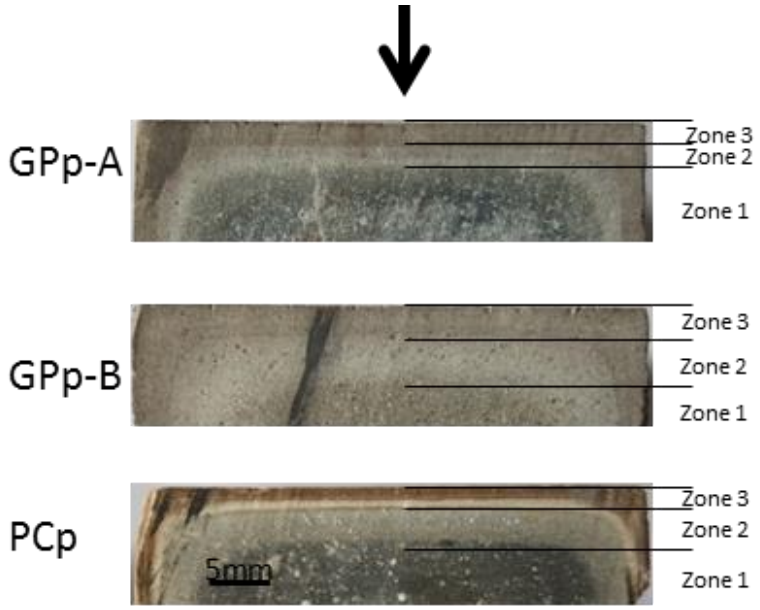

Figure 4: Paste samples showing penetration of silage effluent after 12 months (arrow showing direction of silage effluent penetration)

3.2 Mass loss

The mass loss for the mortar samples over 12 months of exposure to silage effluent is shown in Figure 5. The error bars were determined using the standard deviation of four samples. Initially the samples display similar mass losses, however as time progresses the difference in the mass loss between each sample type increases. After 12 months of exposure the PC samples lost an average of 2.1% of their initial mass. However the GP-A and GP-B only lost 1.6 and 1.1% of their initial mass respectively. The difference in the two GP samples is the percentage of PFA and GGBS in the binder which is shown in Table 2. The binder consisting of 60% PFA and 40% GGBS (GPm-B) displayed a better performance with a mass loss of only 1.1% compared with 1.6% for the samples with a binder consisting of 30% PFA and 70% GGBS (GPm-A).

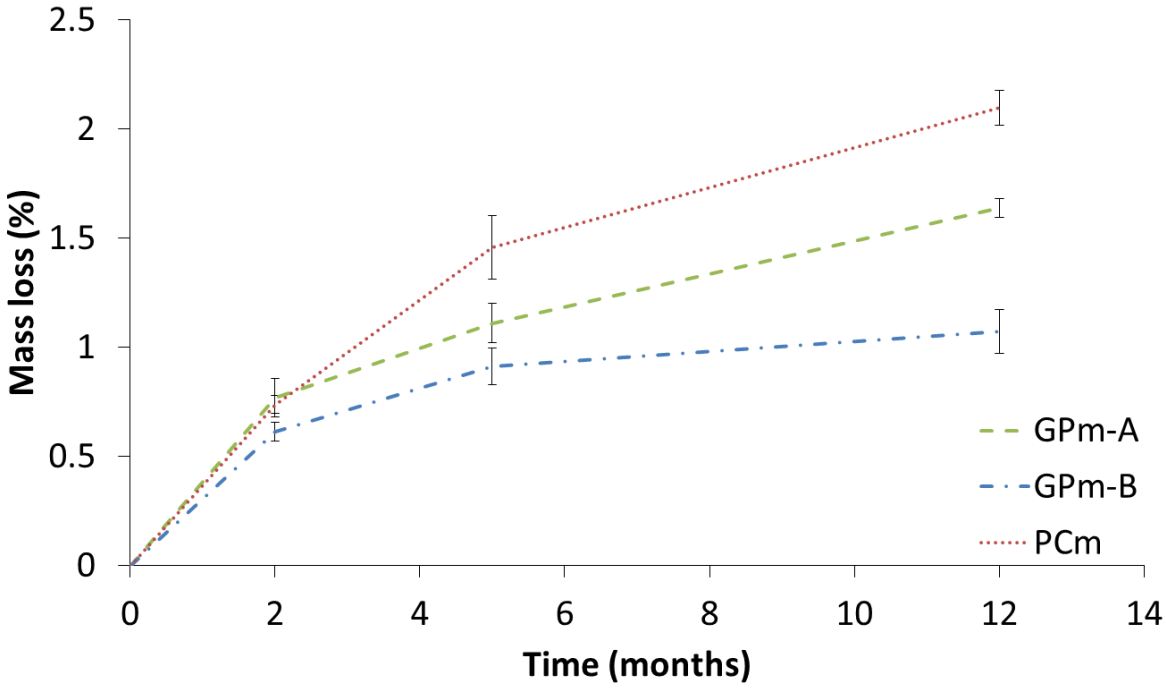

Figure 5: Mass loss (%) of GP and PC mortars after 12 months submersion in silage effluent

3.3 Compressive strength loss

The control samples which were submerged in water for 2 months after normal curing were used as a reference to compare with the samples submerged in silage effluent for 2 and 12 months (Figure 6). The error bars were calculated using the standard deviation from 4 samples and the percentage compressive strength losses are also shown in Figure 6. The compressive strength of the control samples was 81.5, 63.5 and 70 MPa for GPm-A, GPm-B and PCm respectively. After 2 months of submersion in silage effluent GPm-A displayed no change in strength, however after 12 months a 13% strength loss was recorded. For GPm-B an average strength loss of 9% was displayed after both 2 and 12 months. This is in agreement with the mass loss (Figure 5) where only a small further mass loss is recorded after 2 months for GPm-B when compared with the other samples. Another factor may be that the samples internal core continued to develop strength, which was able to offset the loss of mechanical strength at the attacked layer. The PC samples suffered the largest percentage strength loss after both 2 and 12 months losing 17 and 21% respectively when compared with the control sample. This is in agreement with the mass loss (Figure 5) where the PC samples also suffered larger mass losses when compared with both GP samples. These results suggest that GP mortars are more resistant to silage effluent attack than PC mortars.

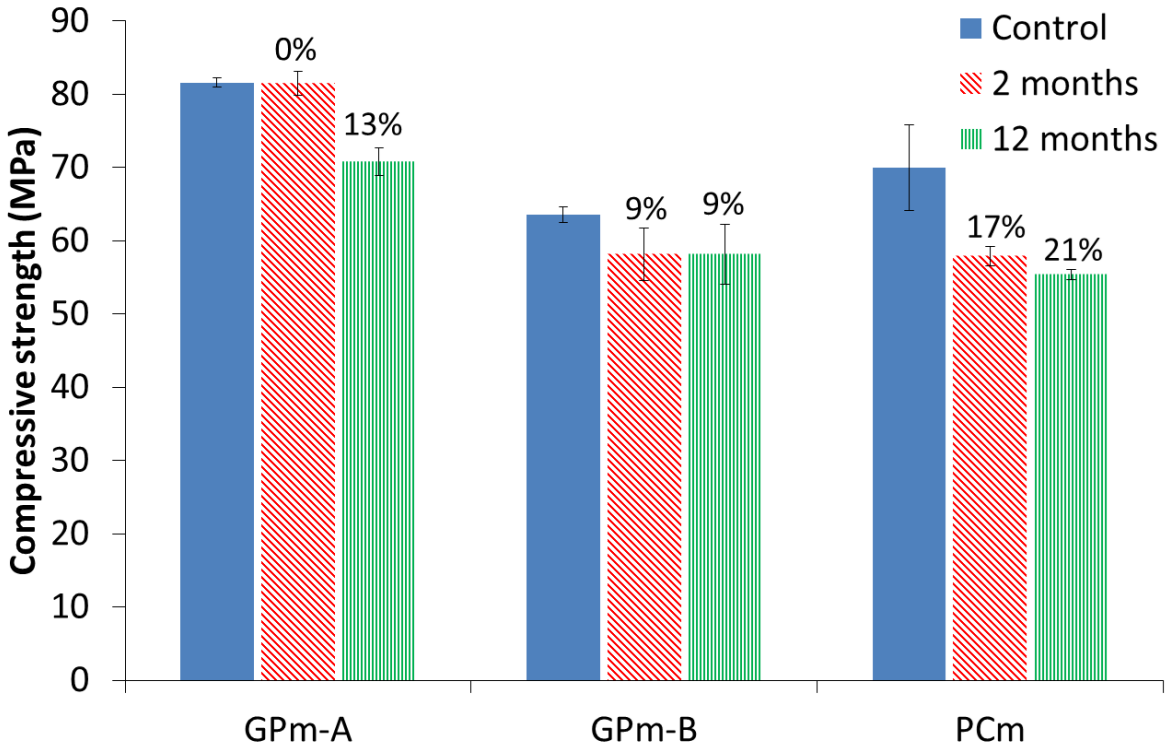

Figure 6: Compressive strength of GP and PC control samples and after 2 and 12 months submersion in silage effluent

3.4 X-ray diffraction (XRD)

As previously mentioned in section 2 powdered samples from the outside layer and the centre of each paste sample were compared. The outside layer of the samples was in direct contact with the silage effluent whereas the centre of the samples was not. Figure 7 shows the XRD spectra for samples GPp-A, GPp-B and PCp after 2 and 12 months of silage effluent submersion. In both GP samples the main peaks identified are Quartz (Q) and Mullite (M). These crystalline phases are present due to unreacted PFA particles which remain embedded after activation [38]. They remain and appear unaffected by the silage effluent attack. A large broad peak is identified at approximately 29^{o} which has been reported to be poorly crystalline C-S-H (calcium silicate hydrate) type gel [39] and can be difficult to identify [40]. This C-S-H gel type varies according to its calcium/silica ratio [41]. In this case it is likely to be calcium aluminium silicate hydrate (C-A-S-H) or sodium aluminium silicate hydrate (N-A-S-H) gel or a coexistence of both called sodium calcium aluminium silicate hydrate (N-C-A-S-H) gel [42]. Significantly this peak has been removed at the outer surface of both GP mixes suggesting the effluent attack has caused decalcification of the main binder gel and a release of sodium and aluminium into the effluent solution.

The XRD spectra of PCp identifies calcium hydroxide, C-S-H, ettringite and AFm phases at the centre of the cube after both 2 and 12 months [43] and [44]. AFm is shorthand for a family of hydrated calcium aluminate phases including monosulphate, hemicarbonate and monocarbonate [45] and [46]. At the edge of the cubes attacked by silage effluent these phases were not present. Calcite (calcium carbonate) was identified instead and after 2 months brushite was also identified. The PC samples have many phases which are vulnerable to silage effluent attack compared with GP samples. This is a significant advantage for GP samples as the removal of these phases leaves behind pore space which allows further ingress of silage effluent.

The formation of an additional compound was evident on the outside surface of PCp as discussed earlier and shown in Figure 3. This compound was identified as brushite which is a phosphate mineral also known as calcium hydrogen phosphate hydrate. It is considered to be a phosphate analogue of calcium sulphate (i.e. gypsum). Phosphate is a component of silage effluent (Table 4) and has reacted with leaching calcium from the cement paste to form brushite.

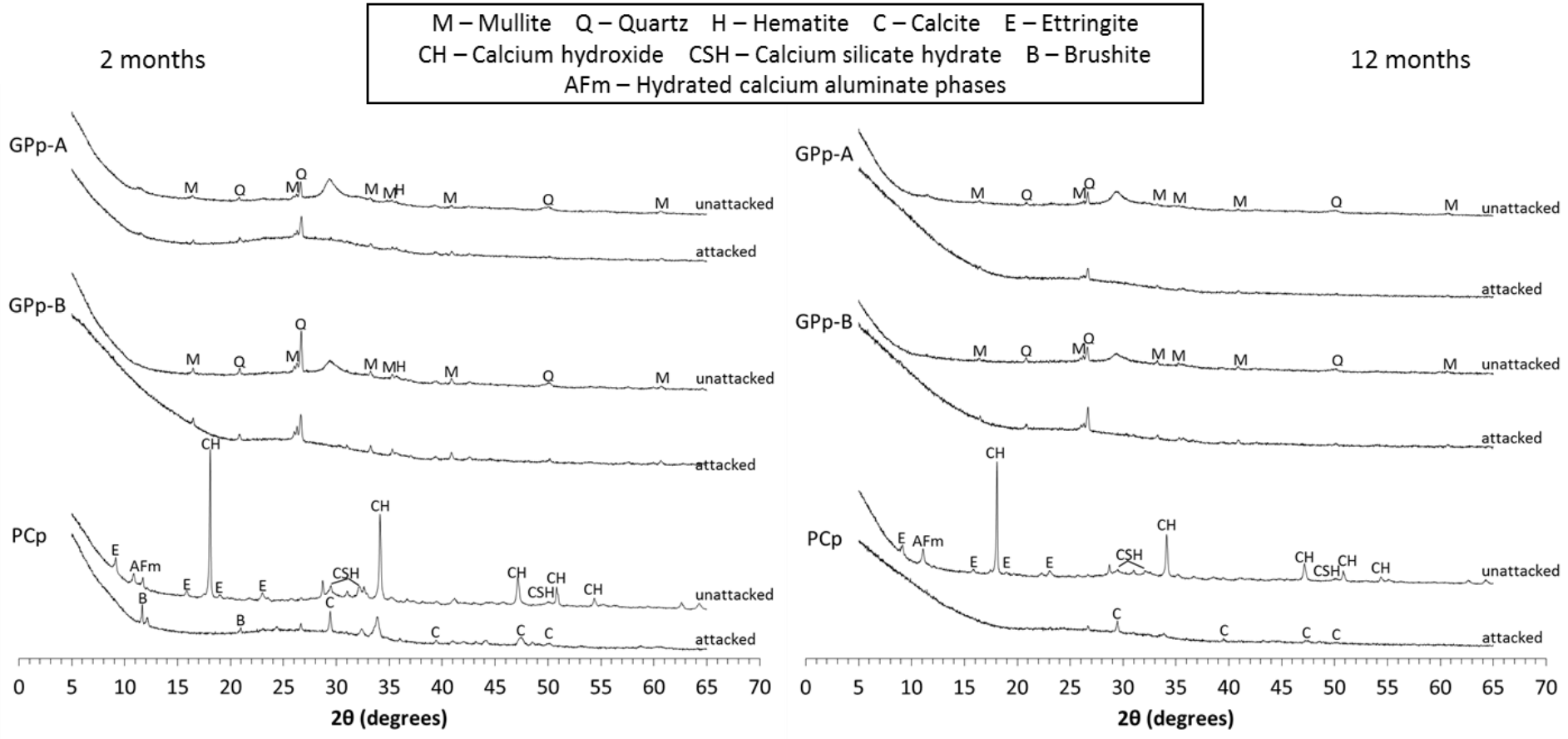

Figure 7: XRD spectra for GPp-A, GPp-B and PCp after 2 (left) and 12 (right) months submersion

3.5 Thermogravimetric analysis (TGA)

Figure 8 shows the differential thermograms (DTG) for samples GPp-A, GPp-B and PCp after 2 and 12 months of silage effluent submersion. The solid line represents the centre of the sample which has not been attacked by the silage effluent and the dashed line represents the outside layer of the sample which has been attacked by the silage effluent.

The alkali activation of PFA and GGBS blends are known to produce a system containing both C-A-S-H and N-A-S-H gels [42]. Furthermore N-C-A-S-H gel may be a hybrid type phase of these gels formed in PFA and GGBS systems [41]. Bound water within the gel structure is removed between 30 and 650 ^{o}C [47]. However the evaporable water is generally considered to be completely eliminated at 120 ^{o}C [48]. For samples GPp-A and GPp-B the main peak occurs at approximately 100 ^{o}C (Figure 8). This peak represents evaporable water and is also attributed to the presence of the main binder gel which has a weight loss between 50 and 200 ^{o}C [49]. This gel type may vary for different sample types depending on the calcium, sodium, silicon and aluminium content as described above. Figure 8 gives the temperature at which the main peak occurs for the GP samples. In the centre of the cubes the peak is centred at higher temperatures after 12 months for both GPp-A and GPp-B compared with 2 months. This suggests that as more gel develops the peak occurs at higher temperatures because the water is more tightly bonded within the gel formed. The peak temperatures are also higher for GPp-A compared with GPp-B suggesting there is also more gel present in GPp-A at both 2 and 12 months and higher temperatures are required to release the more tightly bonded water. At the edge of the samples after two months submersion in effluent the temperature of the main peaks drops to 96 and 95 ^{o}C for GPp-A and GPp-B respectively. This is likely due to decalcification of the binding gel and the water being less tightly bonded. Furthermore the peak may be more related to evaporable moisture which is removed at lower temperatures. After 12 months the main peak occurs at even lower temperatures of 90 and 92 for GPp-A and GPp-B respectively indicating more of the gel has been attacked and the peak is more representative of evaporable moisture. Between 200 and 600 ^{o}C there is a small broad peak centred at approximately 400 ^{o}C at the edge of the GP samples submerged in silage effluent. This peak does not appear at the centre of the cube which suggests it is related to the silage effluent exposure. This is consistent for all samples shown in Figure 8.

For the PC samples there are three main changes which have been identified between the centre and outside layer of the cubes submerged in silage effluent:

- Leaching of calcium hydroxide at the outside layer of the cubes. Dehydroxylation of calcium hydroxide takes place between 450 and 550 ^{o}C [48]. At the centre of PCp after both 2 and 12 months calcium hydroxide can be identified by peaks at 465 and 460 ^{o}C. However at the outside layer of PCp this peak is not present indicating a lack of calcium hydroxide. The calcium hydroxide has been attacked by the silage effluent causing dissolution and leaching of calcium into the silage effluent solution. The dissolution of calcium hydroxide results in an increased porosity and contributes to a decrease in compressive strength[50].
- Decalcification of C-S-H similar to the decalcification of the main binder gel in GP as discussed above. Figure 8 gives the temperature at which the main peak occurs at 2 and 12 months in the centre and at the outside layer of each sample. At the outside layer the peak occurs at lower temperatures suggesting that it is more related to evaporable moisture and a portion of C-S-H has suffered decalcification. The decomposition of ettringite takes place at temperatures between 110 and 170 ^{o}C [48] or more specifically between 104 and 114 ^{o}C [51]. Therefore ettringite may also be decomposed within the temperature range of this peak. Ettringite is a

calcium aluminium sulphate mineral and therefore the attack is similar to calcium hydroxide whereby calcium undergoes dissolution and leaches into the silage effluent solution.

- Removal of AFm phases at the edge of the cubes. A mass loss at approximately 150 ^{o}C indicates the presence of AFm phases [43] and [52] and after increased curing duration this mass loss occurs at higher temperatures [53]. Therefore the mass losses displayed at 157 and 165 ^{o}C at the centre of PCp after 2 and 12 months respectively are related to the presence of AFm phases. These peaks are removed at the edge of the cubes suggesting they have been attacked by the silage effluent exposure.

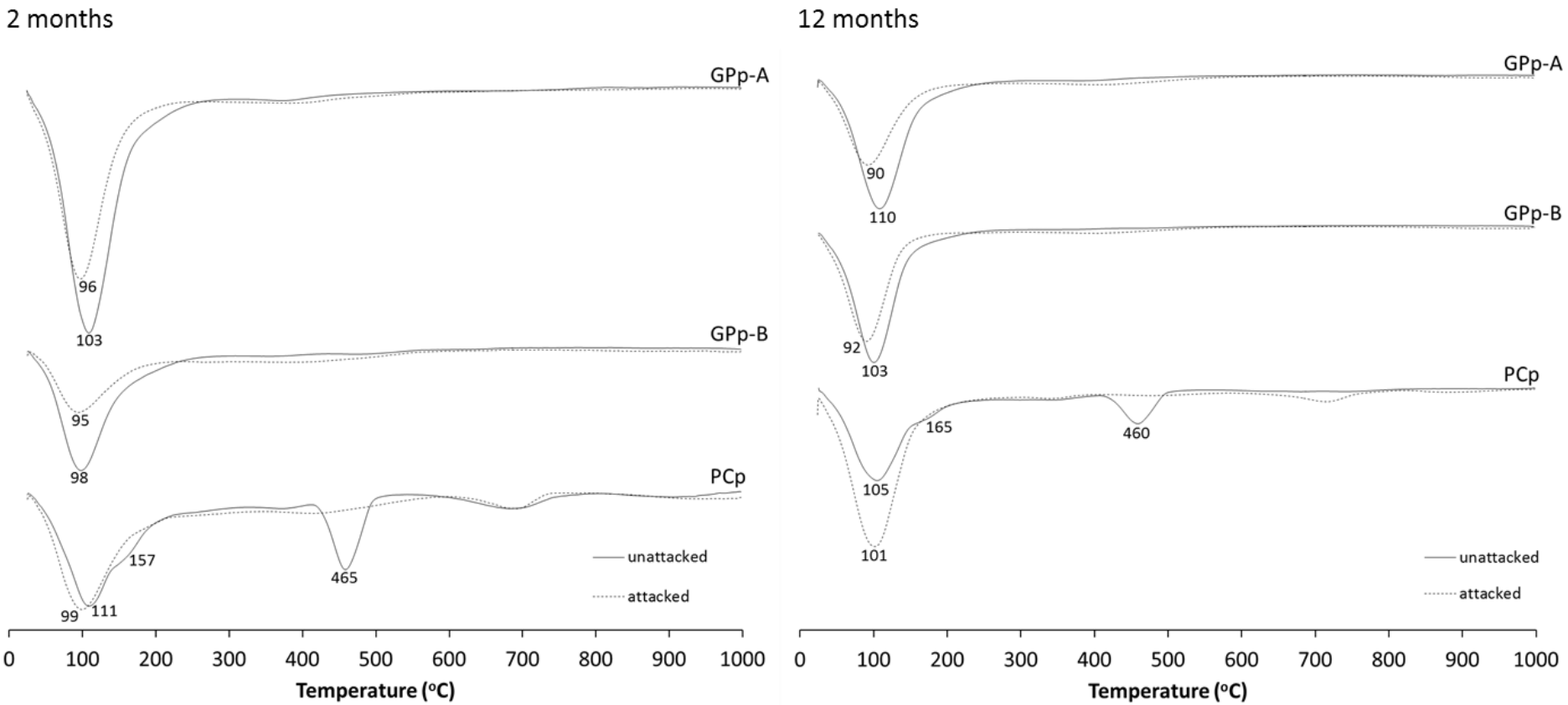

Figure 8: DTG curves for GPp-A, GPp-B and PCp after 2 (left) and 12 (right) months submersion

3.6 Fourier transform infrared spectroscopy (FTIR)

The FTIR spectra of samples GPp-A, GPp-B and PCp is presented in Figure 9 after 2 and 12 months of silage effluent submersion. The solid line represents the centre of each sample and the dashed line represents the outside layer which was attacked by the silage effluent. The following observations have been made from the FTIR spectra data:

- The strongest vibration appears between 944 and 966 cm^{-1} for the samples taken from the centre of the cubes. This broad intense band is assigned to asymmetrical Si-O-Al stretching vibrations [54]. This band is considered to represent C-S-H type gels [26]. This peak shifts to a higher wavenumber between 1024 and 1041 cm^{-1} when the samples are attacked by silage effluent. This shift to higher wave numbers is identified for both the GP and PC samples. This is likely due to decalcification of the main binder gel which leaves a more polymerised gel with lower calcium content in the case of GP samples [55]. In the case of PC the decalcification of C-S-H results in dissolution of calcium, leaving behind a porous corroded layer [56]. Bernal *et al.* (2013) [26] reported that the extent of the structural damage to the binding gel can be identified by the extent of the shift to higher wavenumbers and by the change in intensity of the bands. In the case of GPp-A and GPp-B the shift to higher wavenumbers after 12 months submersion was by 72 and 75 cm^{-1} respectively which is similar to the shift of 76 cm^{-1} in the case of PCp. However when we compare the intensity of the bands each sample provided different changes of intensity when attacked by effluent. The GP samples displayed the smallest change in intensity which was approximately 9 times greater for PCp when compared with GPp-A. This suggests that although decalcification of the C-S-H type gel has taken place in all samples the extent of the structural damage to the binding phase is much lower in GP samples when compared with PC samples [26].
- The formation of a band at 1556 cm^{-1} due to C-O stretching vibrations of calcium acetate is evident in PCp after 12 months [57]. This band is only present at the edge of the PCp samples in contact with the effluent. Calcium acetate is a calcium salt of acetic acid and acetic acid is one of the main constituents of silage effluent [5], therefore the formation of calcium acetate may be possible. However previous research has stated that calcium acetate is highly soluble and therefore unlikely to form in these conditions [58].
- In PCp a narrow band at 3640 cm^{-1} was identified at the centre of the sample but was not present at the outside layer suggesting it has been removed due to the effluent attack. This band is associated with the stretching vibrations in calcium hydroxide [59]. This is consistent with the results of TGA and XRD showing removal of calcium hydroxide due to silage effluent attack.
- The absorption bands at approximately 1650 and 3450 cm^{-1} are due to the stretching vibrations and deformation vibrations of OH and H-O-H groups from water molecules [60].
- The shifting of the shoulder at 1103 (2 months) and 1105 (12 months) to 1170 cm^{-1} in PCp can be associated to the consumption of ettringite [26]. These peaks occur after both 2 and 12 months at similar wavenumbers. The removal of ettringite due to silage effluent attack is consistent with findings from XRD and TGA.

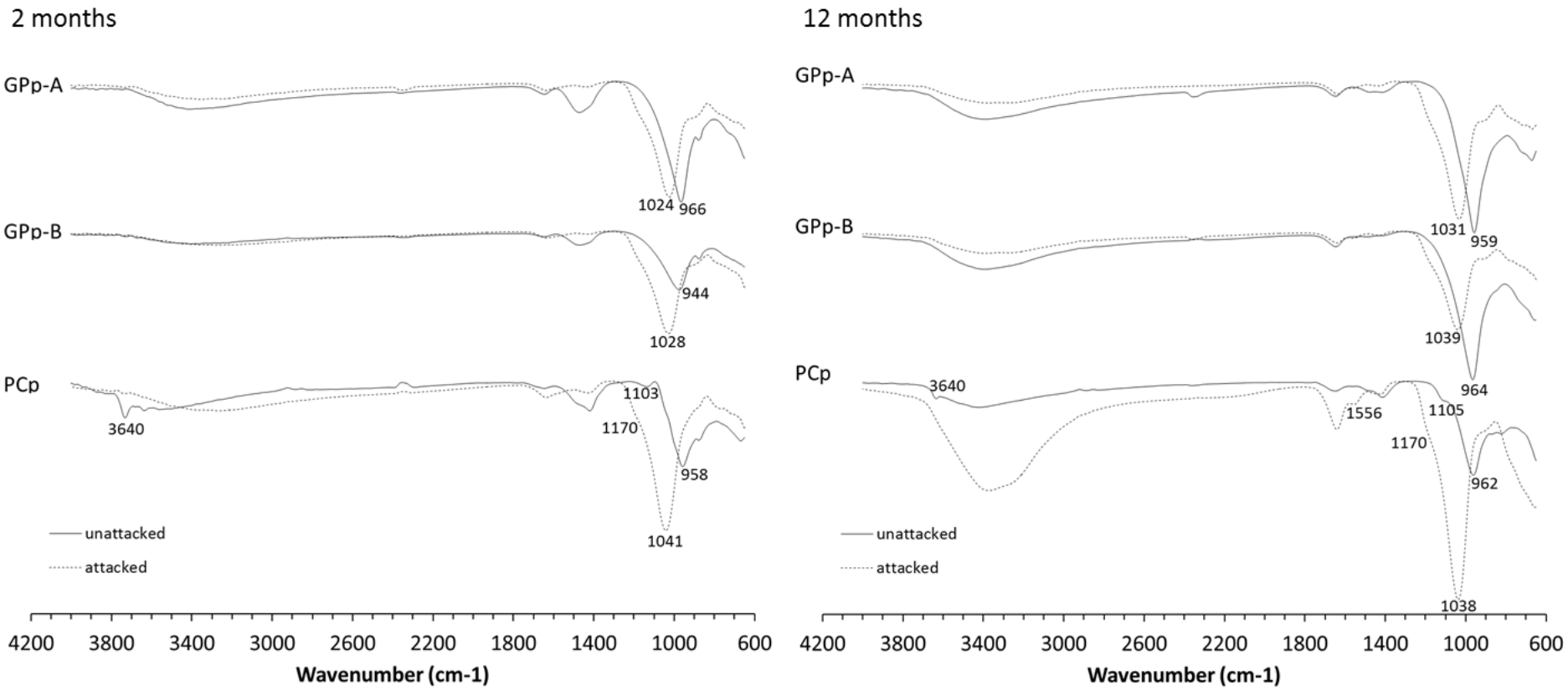

Figure 9: FTIR spectra for GPp-A, GPp-B and PCp after 2 (left) and 12 (right) months submersion

3.7 Scanning electron microscopy (SEM)

SEM images of GPp-A and GPp-B taken from the centre of the pastes after 12 months are shown in Figure 10. After 12 months many of the PFA and GGBS grains have reacted and formed part of the binding gel. However there are still many unreacted or partially reacted particles observed. The unreacted PFA particles are well rounded and the GGBS particles have more irregular shapes. The partially reacted GGBS particles have a light grey centre and darker rims around the edge which indicates they are partially reacted. GPp-A has a higher GGBS content (70%) and GPp-B has a higher PFA content (60%) therefore more GGBS particles can be observed in Figure 10a and more PFA particles can be observed in Figure 10b. Small black voids or cavities can be observed inside or near to PFA particles indicating a more porous microstructure in GPp-B due to higher PFA content. The binding gel between particles seems denser in GPp-A due to lower PFA content.

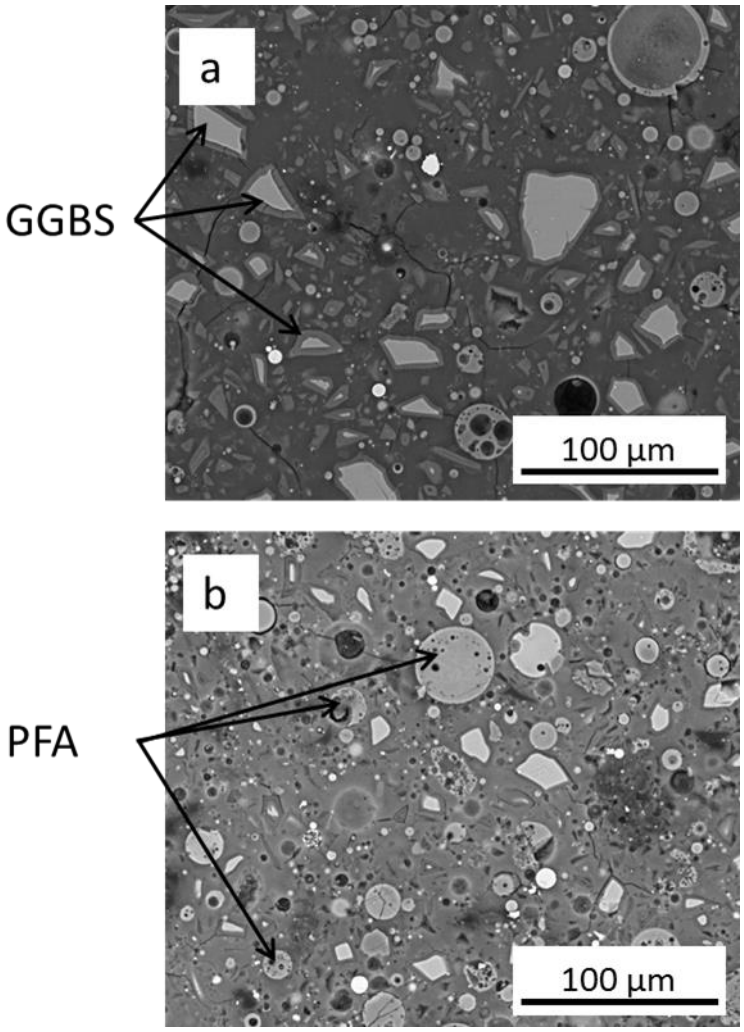

Figure 10: SEM images of a) GPp-A and b) GPp-B after 12 months not attacked

Figure 11 displays the paste samples after 12 months of submersion in silage effluent. The outside edge is shown at the bottom of each image. It is clear from these images that GPp-A and GPp-B have suffered less damage than PCp as a result of the silage effluent submersion. In PCp the edge of the sample has broken down and some paste has been removed. There are also many cracks present which suggest PCp would have continued to suffer deterioration if exposure to silage effluent continued. GPp-A and GPp-B display a more compact microstructure with less breakdown and loss of paste at the sample edge. There are also fewer cracks present when compared with PCp. The microstructure and integrity of the

degraded layer is important for acid resistance because it determines the ability of this layer to remain a protective barrier during further attack [61]. The degraded layers on the GP samples appear much more likely to resist further attack due to the presence of fewer cracks and voids.

Energy dispersive X-ray (EDX) data has been collected from multiple points in the centre and outside layers of the GP and PC samples. The points were selected in the regions of binder gel to avoid unreacted PFA, GGBS and PC particles. Table 5 shows the calcium/silicon and aluminium/silicon ratio at the centre and outside layer of GPp-A, GPp-B and PCp. Each value has been averaged from a minimum of 10 points and the standard deviation is shown in brackets. The Ca/Si ratio at the centre of GPp-A is 1.12 suggesting the existence of C-A-S-H gel. The Ca/Si ratio at the centre of GPp-B is 0.88 suggesting there may be coexistence of C-A-S-H and N-C-A-S-H gel in this sample[42]. The Al/Si ratio at the centre of GPp-A and GPp-B is 0.26 and 0.35 respectively. This is due to GPp-B having a higher PFA content and PFA having a higher aluminium content compared with GGBS. These values are similar with those in literature [42], [62] and [63]. At the outside layer of each sample the Ca/Si ratio is greatly reduced due to silage effluent attack. This is believed to be caused by decalcification of the binding gel. GPp-B appears to be more stable as the reduction of the Ca/Si is much smaller (0.88 to 0.51) compared to GPp-A (1.12 to 0.15). The increased stability of GPp-B may be due to a higher Al/Si ratio of 0.35 compared with 0.26 for GPp-A. Gels with higher aluminium content are more intensely cross-linked and are more resistant to decalcification [55]. This explains why there is a greater mass loss and strength loss after 12 months for GPp-A compared with GPp-B as reported in sections 3.2 and 3.3.

The PC sample has a Ca/Si ratio of 2.89 at the centre as shown in Table 5 which is significantly larger than for both GP samples. At the outside layer which has been attacked this ratio is reduced to 0.44 which is a significantly larger decrease than for both GP samples. This indicates than the C-S-H gel present in PC samples is extremely vulnerable to silage effluent attack due to the higher calcium content when compared with the main binding gel in GP samples. The Al/Si ratio in the centre of the PC samples (0.08) is also lower than the GP samples (0.26 and 0.35) and as discussed above gels with a higher aluminium content are more resistant to decalcification [55].

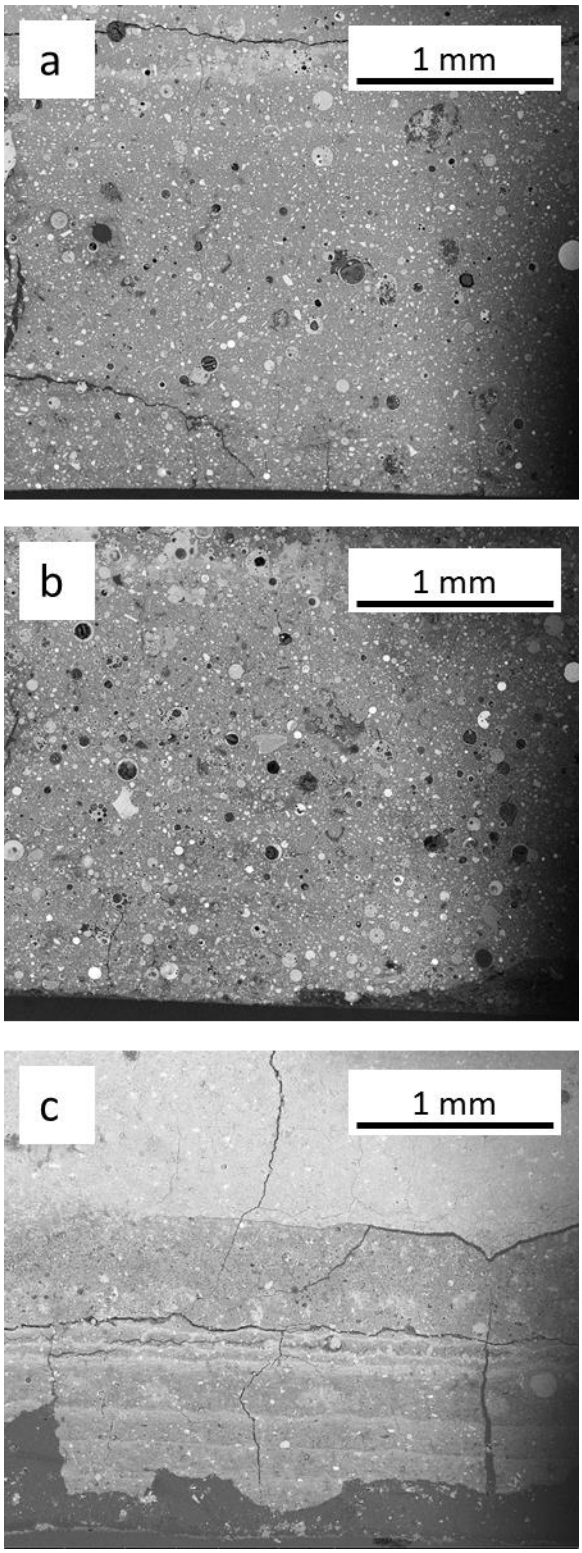

Figure 11: SEM images of silage effluent attack on a) GPp-A, b) GPp-B and c)PCp after 12 months submersion

Table 5: Ca/Si and Al/Si atomic mass ratios from EDX analysis (standard deviation shown in brackets)

Sample name and sampling position	Ca/Si	Al/Si
GPp-A centre	1.12 (0.05)	0.26 (0.03)
GPp-A outside layer	0.15 (0.02)	0.28 (0.03)
GPp-B centre	0.88 (0.07)	0.35 (0.01)
GPp-B outside layer	0.51 (0.02)	0.33 (0.02)
PCp centre	2.89 (0.18)	0.08 (0.01)
PCp outside layer	0.44 (0.04)	0.22 (0.01)

4. Conclusions

This paper has presented the results and discussion of an experimental study conducted to investigate and compare the resistance of GP and PC systems to silage effluent attack. From the comparison of GP and PC systems we can conclude the following.

(1) The mass loss for both GP samples is smaller than that for PC during 12 months of exposure to silage effluent suggesting that GP mortars have increased silage effluent resistance when compared with PC samples. Furthermore SEM images displayed the fragile outside layer on the PC sample compared with the more compact outside layer on the GP samples after 12 months submersion in silage effluent.

(2) The compressive strength of PC samples was found to reduce by 21% after 12 months exposure to silage effluent compared to 13 and 8.5% for the GP samples. This would suggest that GP mortars have increased silage effluent resistance when compared with PC mortars.

(3) XRD, TGA and FTIR were all able to demonstrate the dissolution of calcium hydroxide from the PC samples after silage effluent exposure. The removal of ettringite and AFm phases was also observed. The removal of these phases leaves pore spaces as shown by SEM which increases porosity and allows further ingress and attack by silage effluent. In the case of the GP samples none of these phases were observed which is an advantage because they are susceptible to silage effluent attack.

(4) Both the PC and GP samples suffered decalcification of their main binding gel (C-S-H and C-A-S-H/N-A-S-H) due to silage effluent attack. However the gel in PC appears less stable than the gel in GP samples when attacked by silage effluent. This is due to the higher calcium content highlighted by the higher Ca/Si ratio in PC (2.89) compared with GP (1.12 and 0.88) samples. Furthermore the Al/Si ratio was lower for PC (0.08) when compared with GP (0.26 and 0.35) samples. Gels with higher aluminium content are more intensely crosslinked and therefore more resistant to decalcification [55].

In this study a comparison was also carried out between two GP samples with different blends of PFA and GGBS. GP-A consisted of 30% PFA and 70% GGBS and GP-B consisted of 60% PFA and 40% GGBS.

After 2 months GPm-A displayed better silage effluent resistance than GPm-B because there was no loss of strength and the mass losses were similar. The strength loss for GPm-B after 2 months was 8.5%. Between 2 and 12 months the mass loss for GPm-A increased more rapidly than that for GPm-B and after 12 months the strength loss reached 13% whereas the strength loss for GPm-B remained at 8.5%. Therefore after 12 months GPm-B displayed better silage effluent resistance than GPm-A. This can be attributed to the increased Ca/Si ratio in GPp-A (1.12) compared with GPp-B (0.88) due to the higher GGBS content. Furthermore GPp-B also had a higher Al/Si ratio (0.35) compared with GPp-A (0.26) which results in a more stable gel. The reduction of the Ca/Si ratio in the attacked layer is also much smaller for GPp-B which is reduced to 0.46 compared with 0.18 for GPp-A.

The enhanced early performance of GP-A may be due to lower initial porosity as indicated by SEM whereas GP-B likely has a higher initial porosity allowing faster ingress and onset of effluent attack. However in the longer term GP-B shows superior performance because of the nature of the binding gel produced. Therefore systems containing higher proportions of PFA may offer increased long term silage effluent resistance. However more work needs to be done to assess porosity and depth of penetration of silage effluent in these systems.

Acknowledgments
The authors would like to thank Dr. Mark Russell, Queen's University Belfast for his support and technical assistance throughout. We would also like to acknowledge the SUS-CON project, in particular Dr. Raffaele Vinai and Dr. Ali Rafeet for their work done on optimisation of mixes which were used in this study.

References

[1] C. O'Donnell, P. O'Kiely, V. A. Dodd, and M. Richardson, "A study of the effects of silage effluent on concrete: Part 2, Significance of environmental factors," *J. Agric. Eng. Res.*, vol. 60, pp. 93–97, 1995.

[2] S. Pavía and E. Condren, "A study of the durability of OPC vs. GGBS concrete on exposure to silage effluent," *J. Mater. Civ. Eng.*, vol. 20, no. 4, pp. 313–320, 2008.

[3] D. I. Jones and R. Jones, "The effect of crop characteristics and ensiling methodology on grass silage effluent production," *J. Agric. Eng. Res.*, vol. 60, pp. 73–81, 1995.

[4] V. Zivica and A. Bajza, "Acidic attack of cement based materials - a review.," *Constr. Build. Mater.*, vol. 15, no. 8, pp. 331–340, 2001.

[5] C. O'Donnell, V. A. Dodd, P. O'Kiely, and M. Richardson, "A study of the effects of silage effluent on concrete: Part 1, Significance of concrete characteristics," *J. Agric. Eng. Res.*, vol. 60, pp. 83–92, 1995.

[6] E. Gruyaert, P. Van Den Heede, M. Maes, and N. De Belie, "Investigation of the influence of blast-furnace slag on the resistance of concrete against organic acid or sulphate attack by means of accelerated degradation tests," *Cem. Concr. Res.*, vol. 42, no. 1, pp. 173–185, 2012.

[7] A. Bertron and J. Duchesne, "Attack of Cementitious Materials by Organic Acids in Agricultural and Agrofood Effluents," in *Performance of Cement-Based Materials in Aggressive Aqueous Environments*, RILEM Stat., M. Alexander, A. Bertron, and N. De Belie, Eds. Dordrecht: Springer, 2013, pp. 131–173.

[8] M. M. Gebrehanna, R. J. Gordon, A. Madani, A. C. VanderZaag, and J. D. Wood, "Silage effluent management: A review," *J. Environ. Manage.*, vol. 143, pp. 113–122, 2014.

[9] A. Bertron, “Understanding interactions between cementitious materials and microorganisms: A key to sustainable and safe concrete structures in various contexts,” *Mater. Struct.*, vol. 47, pp. 1787–1806, 2014.

[10] S. Larreur-Cayol, A. Bertron, and G. Escadeillas, “Degradation of cement-based materials by various organic acids in agro-industrial waste-waters,” *Cem. Concr. Res.*, vol. 41, pp. 882–892, 2011.

[11] A. Bertron, J. Duchesne, and G. Escadeillas, “Degradation of cement pastes by organic acids,” *Mater. Struct.*, vol. 40, pp. 341–354, 2007.

[12] M. Richardson, V. A. Dodd, J. J. Lenehan, S. Conaty, and P. O. Kiely, “The influence of cement content and water / cement ratio on the durability of portland cement concretes exposed to silage effluent,” *J. Agric. Eng. Res.*, vol. 72, pp. 137–143, 1999.

[13] V. G. Sangarapillai and J. Dumelow, “Rapid assessment of the durability of concrete exposed to silage effluent,” *Farm Build. Prog.*, vol. 114, pp. 15–17, 1993.

[14] S. Tae, C. Baek, and S. Shin, “Life cycle CO2 evaluation on reinforced concrete structures with high-strength concrete,” *Environ. Impact Assess. Rev.*, vol. 31, no. 3, pp. 253–260, 2011.

[15] A. M. M. Al Bakri, H. Kamarudin, M. Bnhussain, I. K. Nizar, A. R. Rafiza, and Y. Zarina, “The processing, characterization, and properties of fly ash based geopolymer concrete,” *Rev. Adv. Mater. Sci.*, vol. 30, pp. 90–97, 2012.

[16] V. Sata, A. Sathonsaowaphak, and P. Chindaprasirt, “Resistance of lignite bottom ash geopolymer mortar to sulfate and sulfuric acid attack,” *Cem. Concr. Compos.*, vol. 34, no. 5, pp. 700–708, 2012.

[17] F. Pacheco-Torgal, Z. Abdollahnejad, A. F. Camoes, M. Jamshidi, and Y. Ding, “Durability of alkali-activated binders: A clear advantage over Portland cement or an unproven issue?,” *Constr. Build. Mater.*, vol. 30, pp. 400–405, 2012.

[18] P. S. Deb, P. Nath, and P. K. Sarker, “The effects of ground granulated blast-furnace slag blending with fly ash and activator content on the workability and strength properties of geopolymer concrete cured at ambient temperature,” *Mater. Des.*, vol. 62, pp. 32–39, 2014.

[19] R. San Nicolas, S. A. Bernal, R. Mejía de Gutiérrez, J. S. J. van Deventer, and J. L. Provis, “Distinctive microstructural features of aged sodium silicate-activated slag concretes,” *Cem. Concr. Res.*, vol. 65, pp. 41–51, Nov. 2014.

[20] C. Ridtirud, P. Chindaprasirt, and K. Pimraksa, “Factors affecting the shrinkage of fly ash geopolymers,” *Int. J. Miner. Metall. Mater.*, vol. 18, no. 1, pp. 100–104, 2011.

[21] UKQAA, “UKQAA Ash Availability Report,” Wolverhampton, 2016.

[22] A. Heath, K. Paine, S. Goodhew, M. Ramage, and M. Lawrence, “The potential for using geopolymer concrete in the UK,” *Constr. Mater.*, vol. 166, no. CM4, pp. 195–203, 2013.

[23] M. Kovtun, M. Ziolkowski, J. Shekhovtsova, and E. Kearsley, “Direct electric curing of alkali-activated fly ash concretes : a tool for wider utilization of fly ashes,” *J. Clean. Prod.*, vol. 133, pp. 220–227, 2016.

[24] T. Bakharev, J. G. Sanjayan, and Y. B. Cheng, “Resistance of alkali-activated slag concrete to acid attack,” *Cem. Concr. Res.*, vol. 33, pp. 1607–1611, 2003.

[25] C. Shi, “Corrosion resistance of alkali-activated slag cement,” *Adv. Cem. Res.*, vol. 15, no. 2, pp. 77–81, 2003.

[26] S. A. Bernal, E. D. Rodríguez, R. M. de Gutierrez, and J. L. Provis, “Performance of alkali-activated slag mortars exposed to acids,” *J. Sustain. Cem. Mater.*, vol. 1, pp. 37–41, 2012.

[27] A. Fernandez-Jimenez, I. García-Lodeiro, and A. Palomo, “Durability of alkali-activated fly ash cementitious materials,” *J. Mater. Sci.*, vol. 42, no. 9, pp. 3055–3065, 2007.

[28] Z. Bascarevic, M. Komljenovic, Z. Miladinovic, V. Nikolic, N. Marjanovic, Z. Zujovic, and R. Petrovic, “Effects of the concentrated NH4NO3 solution on mechanical properties and structure of the fly ash based geopolymers,” *Constr. Build. Mater.*, vol. 41, no. 3, pp. 570–579, 2013.

[29] Y. Liu, W. Zhu, and E.-H. Yang, “Alkali-activated ground granulated blast-furnace slag incorporating incinerator fly ash as a potential binder,” *Constr. Build. Mater.*, vol. 112, pp. 1005–1012, 2016.

[30] A. Buchwald, P. Harpe, S. Schiecke, T. Hagedorn, and B. Leydolph, “Resistance against organic acid attack in fodder fermenting silo - comparison of the performance of OPC and alkali-activated binder based concretes,” in *34th Cement and Concrete Science Conference*, 2014.

[31] British Standards Institution, “BS EN 197-1:2011 - Cement Part 1: Composition, specifications and conformity criteria for common cements,” London, UK, 2011.

[32] British Standards Institution, “BS 812-2:1995 - Testing aggregates. Methods for determination of density,” London, UK, 1995.

[33] A. Rafeet, “Mix design, fresh and hardened properties and microstructural characterization of alkali-activated concrete based on PFA/GGBS blends,” Queen’s University Belfast, 2016.

[34] R. Vinai, A. Rafeet, M. Soutsos, and W. Sha, “The role of water content and paste proportion on physico- mechanical properties of alkali activated fly ash – ggbs concrete,” *J. Sustain. Metall.*, vol. 2, pp. 51–61, 2016.

[35] A. Bertron, J. Duchesne, and G. Escadeillas, “Accelerated tests of hardened cement pastes alteration by organic acids : analysis of the pH effect,” *Cem. Concr. Res.*, vol. 35, pp. 155–166, 2005.

[36] A. Bertron, “Methods for Testing Cementitious Materials Exposed to Organic Acids,” in *Performance of Cement-Based Materials in Aggressive Aqueous Environments*, M. Alexander, A. Bertron, and N. De Belie, Eds. Dordrecht: Springer, 2013, pp. 355–387.

[37] J. L. Provis, R. J. Myers, C. E. White, V. Rose, and J. S. J. van Deventer, “X-ray microtomography shows pore structure and tortuosity in alkali-activated binders,” *Cem. Concr. Res.*, vol. 42, no. 6, pp. 855–864, Jun. 2012.

[38] A. Fernández-Jiménez and A. Palomo, “Mid-infrared spectroscopic studies of alkali-activated fly ash structure,” *Microporous Mesoporous Mater.*, vol. 86, no. 1–3, pp. 207–214, 2005.

[39] A. Fernández-Jiménez, F. Puertas, I. Sobrados, and J. Sanz, “Structure of calcium silicate hydrates formed in alkaline-activated slag: Influence of the type of alkaline activator,” *J. Am. Ceram. Soc.*, vol. 86, no. 8, pp. 1389–1394, 2003.

[40] F. Puertas, A. Fernandez-Jimenez, and M. T. Blanco-Varela, “Pore solution in alkali-activated slag cement pastes. Relation to the composition and structure of calcium silicate hydrate,” *Cem. Concr. Res.*, vol. 34, no. 1, pp. 139–148, 2004.

[41] N. K. Lee, J. G. Jang, and H. K. Lee, “Shrinkage characteristics of alkali-activated fly ash/slag paste and mortar at early ages,” *Cem. Concr. Compos.*, vol. 53, pp. 239–248, Oct. 2014.

[42] I. Ismail, S. A. Bernal, J. L. Provis, R. San Nicolas, S. Hamdan, and J. S. J. Van Deventer, “Modification of phase evolution in alkali-activated blast furnace slag by the incorporation of fly ash,” *Cem. Concr. Compos.*, vol. 45, pp. 125–135, 2014.

[43] B. Z. Dilnesa, B. Lothenbach, G. Le Saout, G. Renaudin, A. Mesbah, Y. Filinchuk, A. Wichser, and E. Wieland, “Iron in carbonate containing AFm phases,” *Cem. Concr. Res.*, vol. 41, no. 3, pp. 311–323, 2011.

[44] L. G. Baquerizo, T. Matschei, K. L. Scrivener, M. Saeidpour, and L. Wadsö, “Hydration states of AFm cement phases,” *Cem. Concr. Res.*, vol. 73, pp. 143–157, 2015.

[45] T. Matschei, B. Lothenbach, and F. P. Glasser, “The AFm phase in Portland cement,” *Cem. Concr. Res.*, vol. 37, pp. 118–130, 2007.

[46] B. Z. Dilnesa, E. Wieland, B. Lothenbach, R. Dähn, and K. L. Scrivener, “Fe-containing phases in hydrated cements,” *Cem. Concr. Res.*, vol. 58, pp. 45–55, 2014.

[47] M. Ben Haha, B. Lothenbach, G. Le Saout, and F. Winnefeld, “Influence of slag chemistry on the hydration of alkali-activated blast-furnace slag - Part I: Effect of MgO,” *Cem. Concr. Res.*, vol. 41, pp. 955–963, 2011.

[48] L. Alarcon-Ruiz, G. Platret, E. Massieu, and A. Ehrlacher, “The use of thermal analysis in assessing the effect of temperature on a cement paste,” *Cem. Concr. Res.*, vol. 35, no. 3, pp. 609–613, 2005.

[49] M. Ben Haha, G. Le Saout, F. Winnefeld, and B. Lothenbach, “Influence of activator type on hydration kinetics, hydrate assemblage and microstructural development of alkali activated blast-furnace slags,” *Cem. Concr. Res.*, vol. 41, no. 3, pp. 301–310, 2011.

[50] C. Carde and R. François, “Effect of the leaching of calcium hydroxide from cement paste on mechanical and physical properties,” *Cem. Concr. Res.*, vol. 27, no. 4, pp. 539–550, 1997.

[51] A. Chaipanich and T. Nochaiya, “Thermal analysis and microstructure of Portland cement-fly ash-silica fume pastes,” *J. Therm. Anal. Calorim.*, vol. 99, pp. 487–493, 2010.

[52] B. Lothenbach, G. Le Saout, E. Gallucci, and K. Scrivener, “Influence of limestone on the hydration of Portland cements,” *Cem. Concr. Res.*, vol. 38, pp. 848–860, 2008.

[53] M. Zajac, A. Rossberg, G. Le Saout, and B. Lothenbach, “Influence of limestone and anhydrite on the hydration of Portland cements,” *Cem. Concr. Compos.*, vol. 46, pp. 99–108, 2014.

[54] T. Bakharev, “Resistance of geopolymer materials to acid attack,” *Cem. Concr. Res.*, vol. 35, pp. 658–670, 2005.

[55] C. Varga, M. M. Alonso, R. Mejía de Gutierrez, J. Mejía, and F. Puertas, “Decalcification of alkali-activated slag pastes. Effect of the chemical composition of the slag,” *Mater. Struct.*, vol. 48, no. 3, pp. 541–555, 2014.

[56] M. Komljenovic, Z. Bascarevic, N. Marjanovic, and V. Nikolic, “Decalcification resistance of alkali-activated slag,” *J. Hazard. Mater.*, vol. 233, pp. 112–121, 2012.

[57] A. W. Musumeci, R. L. Frost, and E. R. Waclawik, “A spectroscopic study of the mineral paceite (calcium acetate),” *Spectrochim. Acta - Part A Mol. Biomol. Spectrosc.*, vol. 67, no. 3–4, pp. 649–661, 2007.

[58] L. De Windt, A. Bertron, S. Larreur-Cayol, and G. Escadeillas, “Interactions between hydrated cement paste and organic acids: Thermodynamic data and speciation modeling,” *Cem. Concr. Res.*, vol. 69, pp. 25–36, 2015.

[59] F. Puertas, M. Palacios, H. Manzano, J. S. Dolado, a. Rico, and J. Rodríguez, “A model for the C-A-S-H gel formed in alkali-activated slag cements,” *J. Eur. Ceram. Soc.*, vol. 31, no. 12, pp. 2043–2056, 2011.

[60] A. Palomo, M. T. Blanco-Varela, M. L. Granizo, F. Puertas, T. Vazquez, and M. W. Grutzeck, “Chemical stability of cementitious materials based on metakaolin,” *Cem. Concr. Res.*, vol. 29, no. 7, pp. 997–1004, 1999.

[61] T. Gutberlet, H. Hilbig, and R. E. Beddoe, “Acid attack on hydrated cement - Effect of mineral acids on the degradation process,” *Cem. Concr. Res.*, vol. 74, pp. 35–43, 2015.

[62] N. K. Lee and H. K. Lee, “Reactivity and reaction products of alkali-activated, fly ash/slag paste,” *Constr. Build. Mater.*, vol. 81, pp. 303–312, 2015.

[63] B. S. Gebregziabiher, R. Thomas, and S. Peethamparan, “Very early-age reaction kinetics and microstructural development in alkali-activated slag,” *Cem. Concr. Compos.*, vol. 55, pp. 91–102, Jan. 2015.